Tutorial: migration imaging conditions

Ian F. Jones[1*]

Abstract

Migration of seismic data is the process that attempts to build an image of the Earth's interior from recorded field data, by repositioning these data into their 'true' geological position in the subsurface, using various numerical approximations of either a wave-theoretical or ray-theoretical description of the propagation of sound waves in the subsurface.

This migration can be described as being performed in a number of stages, both for ray and wave-extrapolation based methods. The final stage of the migration process is that which forms the image, via what is known as an imaging condition. In this tutorial, I will outline the various methods involved in forming imaging conditions, primarily for the case of wave-extrapolation methods, and describe some of the techniques used to build gathers of pre-stack-migrated data for use in post-migration velocity analysis.

Introduction

Migration has been in widespread use as an industrial process since the mid-1970s for 2D post-stack data and since the late 1990s for pre-stack 3D data (e.g. Bancroft 1997, 2007; Jones et al., 2008). Consequently, most geoscientists are familiar with the underlying concepts and the principles embedded in the various migration approaches used in time and depth imaging (e.g. Jones and Lambaré 2003; Williamson et al., 2010), for both the ray-based methods such as Kirchhoff and beam (Popov, 1982; Hill, 1990; Gray 1992, 2004), and to perhaps a lesser extent, the wavefield extrapolation migration (WEM) methods (Hale, 1991). The WEM techniques fall into two broad classes, depending on whether they comprehend vertical changes in direction for the propagating waves: namely one-way wave-equation wavefield extrapolation migration (also often referred to as WEM), and two-way wave-equation reverse-time migration (RTM) (see for example, Hemon, 1978; McMechan, 1983; Whitmore, 1983; Beysal et al., 1983; Bednar et al., 2003).

Perhaps less well understood are the various steps involved in determining how a wavefield propagates through the subsurface (as represented by a velocity-depth model, e.g. Jones, 2010) and the subsequent step of building an image of the associated reflectivity structure of the earth (e.g. Claerbout, 1971; Leveille et al., 2011; Liu et al., 2011). Here, I will be reviewing the latter stages of the imaging process: the so-called imaging condition.

Imaging conditions

To paraphrase Newton, what comes up must have gone down, and in the context of seismic exploration, for there to be an upcoming echo from a subsurface reflector we must have originally had a downgoing sound signal. This notion was formulated in a slightly different way by Jon Claerbout (1971) who noted that if there is a reflector in the subsurface (an impedance contrast), then at that point in space, when the downgoing source wavefield hits the reflector, an upcoming reflection is generated which then travels up to the receivers. In other words, wherever the source and receiver wavefields are in the same place at the same time, there must be a reflector. This observation forms the basis of an imaging condition.

This concept underpins how all migration techniques build an image. For ray theory methods, we perform ray tracing from the surface source locations down into the earth for all desired subsurface image points, and ray trace similarly for the surface receiver locations from subsurface image points. In practice, for single mode propagation, the ray paths are interchangeable for the path between a given surface and subsurface point. For wavefield extrapolation migration methods, we compute the wavefields for all propagation times for both waves emitted at the source location and waves recorded at the receiver position (using finite difference techniques for example). We compute the representative downgoing source wavefield by modelling the response of a specified waveform going into the earth, and at the same time back-propagate the actual recorded real data from their surface receiver positions.

For both of these approaches an image is formed where the downgoing and upcoming wavefields intersect, and in the following sections I will describe these methods in more detail.

The imaging condition for ray methods

In ray-based methods, the migration process is decomposed into two or more stages (Červený, 2001). For Kirchhoff, this entails the calculation of travel times associated with a given velocity model from representative surface source and

[1] *ION-GXT, UK.*
[*] *Corresponding author, E-mail: Ian.Jones@iongeo.com*

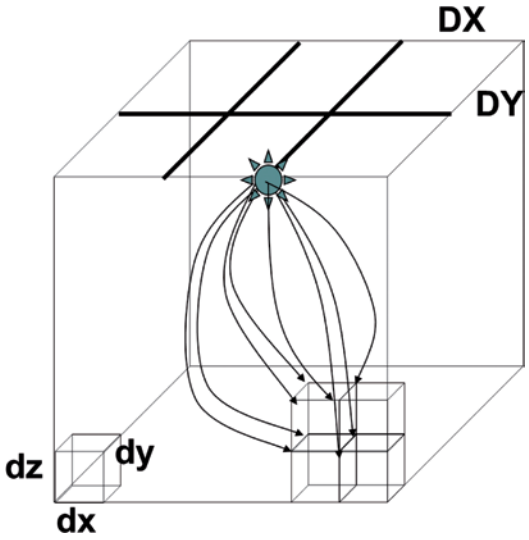

Figure 1 *In ray-based methods, rays are traced through a current velocity model from a surface position sampled on the 2D grid (DX, DY), representing a source or receiver location (as denoted by the star) to a grid of subsurface points on the 3D grid (dx, dy, dz).*

receiver locations to all subsurface points on a predefined grid (Figure 1). This step is typically followed by distribution of input data along the computed surfaces of constant travel time (the isochrones), which represent the transit time from the source to the receiver, via the subsurface reflection point, then summation of contributions resulting from all the input data traces. When a sufficient number of input traces' individual response contributions have been summed, the imaging condition will eventually build up an image of the reflector. Figure 2a shows an early stage in this summation process; we can still discern the individual migration responses. Once the process is complete and all input contributions have been summed, the responses merge to build an image of the reflector (constructive interference) and to cancel the unwanted portions of the responses (destructive interference), as seen in Figure 2b.

For a beam scheme, the travel time computation is preceded with a slope field determination (typically using a slant stack analysis of shot, receiver, or offset gathers), which facilitates selection of only those travel paths that will meaningfully contribute to the image. In this case, ideally the imaging condition is restricted to the Fresnel zone in the vicinity of the reflector (Popov, 1982; Hill, 1990).

In both the Kirchhoff and beam methods, the step which forms the image (the imaging condition) is essentially the summation of all contributions resulting from the input data traces after they have been spread along portions of the various isochrones. In other words, we rely on the principle of constructive and destructive interference (stationary phase) to form the image.

In ray-based methods, the procedure can be performed for each trace at a time, and also, the image can be formed for localized subsets of the final image. This feature makes ray-based methods cost effective (thus desirable) for iterative velocity model updating. A corollary of this observation is that surface-offset gathers can easily be computed, rather than just a final (stacked) image: which is a requirement for velocity analysis. Surface offset gathers can be later converted to angle gathers, or in beam schemes and Kirchhoff variants such as common reflection angle migration (Koren et al., 2007) angle gathers can be formed directly.

The tracing of rays though a velocity model, in advance of forming the image, has both advantages and disadvantages. The advantage, just mentioned, is that subsets of the migrated data can be cost-effectively computed by ray tracing for only

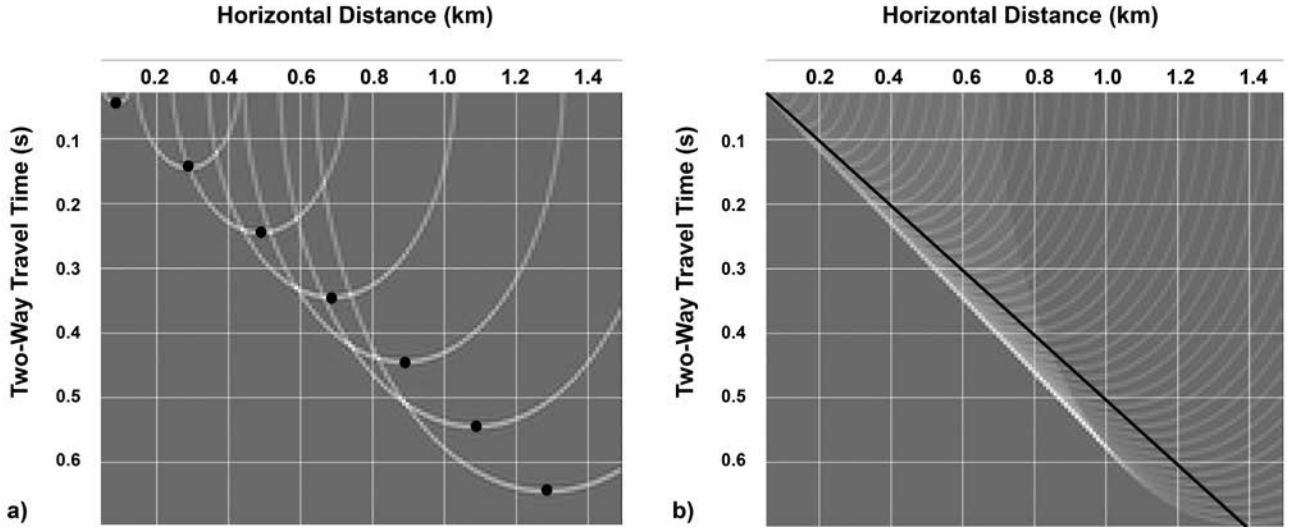

Figure 2 *The imaging condition for ray-based methods. a) For each input trace (with a contributing wavelet represented by the black dots), a migration response is formed and added to the output image space (whether it be time or depth). b) When enough elemental responses are added, eventually an image of the reflectors builds up and the superfluous parts of the responses tend to cancel-out. The solid black line shows the locations of the input trace wavelets (the dots in Figure 2a), and the white line formed by the superposition of responses (the tangential envelope) which is the output migrated result (Figure from Jones et al., 2008).*

the parts of interest (whether they be gathers or subsets of the image). The disadvantage is that the formation of the image is decoupled from the velocity model via the travel-time representation of the wave behaviour in the earth. This decoupling introduces an undesirable resampling of information (converting velocity to equivalent representative travel times) often on a much coarser grid than the velocity was sampled at. Additionally, during the subsequent formation of the image, this travel time information has to be interpolated back from the sample grid on which it is stored, to the grid on which we require the image. This has to be done to estimate the travel times we would have from the actual source and receiver locations by using those values we computed on the coarse surface grid (DX, DY in Figure 1), and also for the desired output migrated samples (typically on a 12.5 m x 12.5 m x 5 m grid) given those we computed at spacing dx, dy, dz (in Figure 1): typically 100 m x 100 m x wz (where wz is less than the water depth for marine data). In addition, using a ray to represent a wave also limits our inherent resolution to the size of the Fresnel zone (as in ray theory we are asserting that every ray is totally independent of any neighbouring ray, whereas for real waves this is untrue within the Fresnel zone).

The imaging condition for wavefield extrapolation methods

Wavefield extrapolation migration of shot records involves extrapolation of a synthetic source wavefield down into the earth (downward continuation), and at the same time, extrapolation of the actual real recorded wavefield back from the receivers into the earth (called upward continuation, as we move energy back towards the source).

Referring back to Claerbout's imaging condition mentioned earlier, for a wavefield extrapolation migration we can build an image by multiplying the source and receiver wavefields together at each propagation time step, and where we have a high amplitude contribution resulting from this product, there must have been a reflector in the subsurface. At each propagation time-step, the source-side and receiver-side 3D wavefields are multiplied together, and at the end of the extrapolation process (when we have exhausted all the useful propagation time) all these hundreds of 3D product volumes are summed together to form the image contribution resulting from this particular shot record.

This summation of wavefield products is referred to as the correlation imaging condition in shot migration: the image is being formed by what is essentially a correlation of downgoing and upcoming wavefields (e.g. Bancroft, 1997). This process is repeated for all available shots, and all these overlapping 3D shot-contribution volumes are summed to form the full migrated image of the study area. Figure 3a is a cartoon depicting the underlying correlation imaging condition for a shot migration, and Figure 3b depicts a synthetic modelling exercise showing the superposition for the downgoing and upcoming wavefields for a single shot, as well as the resulting image after summing all shots (Figure 3c).

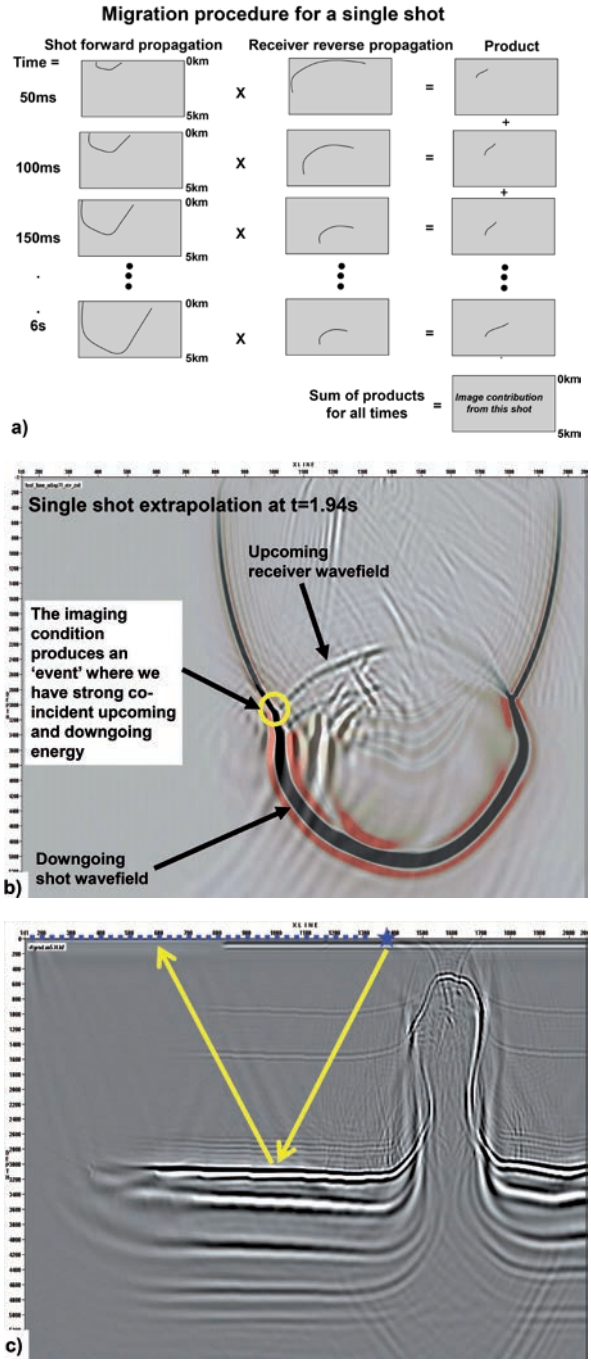

Figure 3 *a) At each propagation time step, the downgoing and upcoming (source and receiver) wavefields are multiplied, and then all these 3D product volumes are summed to make the image contribution for this input 3D shot gather. This cartoon is a bit misleading, as although the source-side wavefield is computed starting from time=0 in small propagation steps up to the maximum recording time, the corresponding receiver-side back propagation is done in reverse: from time=Tmax, back to time=0. Hence, all the receiver-side time-movie snapshots must first be computed, then reversed in order, prior to multiplication with the corresponding source-side movie frames (although there are various computation tricks to save memory while doing this). b) A synthetic modelling exercise showing the superposition for the downgoing and upcoming wavefields for a single shot for propagation time 1.94s: the red-and-black event is the downgoing source contribution, and the black-and-white overlay is the upcoming receiver wavefield. c) The resulting image after summing all shots for all time steps: the yellow ray-path denotes the reflection point corresponding to the yellow circle indicated in 3b.*

However, this summation of image contributions for all propagation time results in an image, and not a gather of pre-stack traces. There is no pre-stack gather information associated with such shot migration schemes. Hence, if we need gathers for post-migration velocity update (Zhou et al., 2011), we have to introduce a method for forming them.

1D convolutional model analogy

In the 1D convolution model of reflection seismology, we note that the recorded signal is equal to the Earth's reflectivity response convolved with the downgoing source wavelet. In the context of the current discussion, the recorded signal is the upcoming wavefield as measured at the receivers on the surface, and the source is the downgoing wavefield. So, we have:

$$\text{Upcoming} = \text{Downgoing} * \text{Reflectivity} \quad (1)$$

In order to estimate the reflectivity in this 1D case, we perform some form of trace-by-trace deconvolution, essentially 'dividing' by the recorded upcoming signal by the downgoing source wavelet term:

$$\text{Reflectivity} = \text{Upcoming} / \text{Downgoing} \quad (2)$$

However, in implementing the shot migration imaging condition, as described in the previous section, we are performing a multiplication of the upcoming and downgoing 3D wavefields:

$$\text{Reflectivity} = \text{Upcoming} * \text{Downgoing} \quad (3)$$

As described in equation (2) we should actually be dividing these two terms (division in the frequency domain or deconvolution in the time domain). In other words, in the tradition of all good geophysicists, we take the liberty of making the approximation that division can be replaced by multiplication! In order to recover from this embarrassing approximation, and atone for other sins, we can divide the product in equation (3) by the square of the downgoing wavefield (plus a small constant, epsilon, to help avoid division by zero).

$$\text{Reflectivity} = (\text{Upcoming} * \text{Downgoing}) / (\text{Downgoing}^2 + \text{epsilon}) \quad (4)$$

The reason for trying to avoid performing this division directly is that small terms in the denominator lead to numerical instability, so the multiplication trick allows us to see where we have a subsurface reflector (in accordance with Claerbout's imaging principle). The subsequent division in equation (3) attempts to balance the amplitudes. This latter division is referred to as illumination compensation (e.g. Schleicher et al., 2007; Liu et al., 2007).

We can try to form this imaging condition more correctly with a form of inversion or deconvolution (a least-squares or deconvolutional imaging condition, e.g. Schuster, 1997; Nemeth et al., 1999; Guiton et al., 2006), but this tends to be very expensive, so is not currently in widespread industrial use.

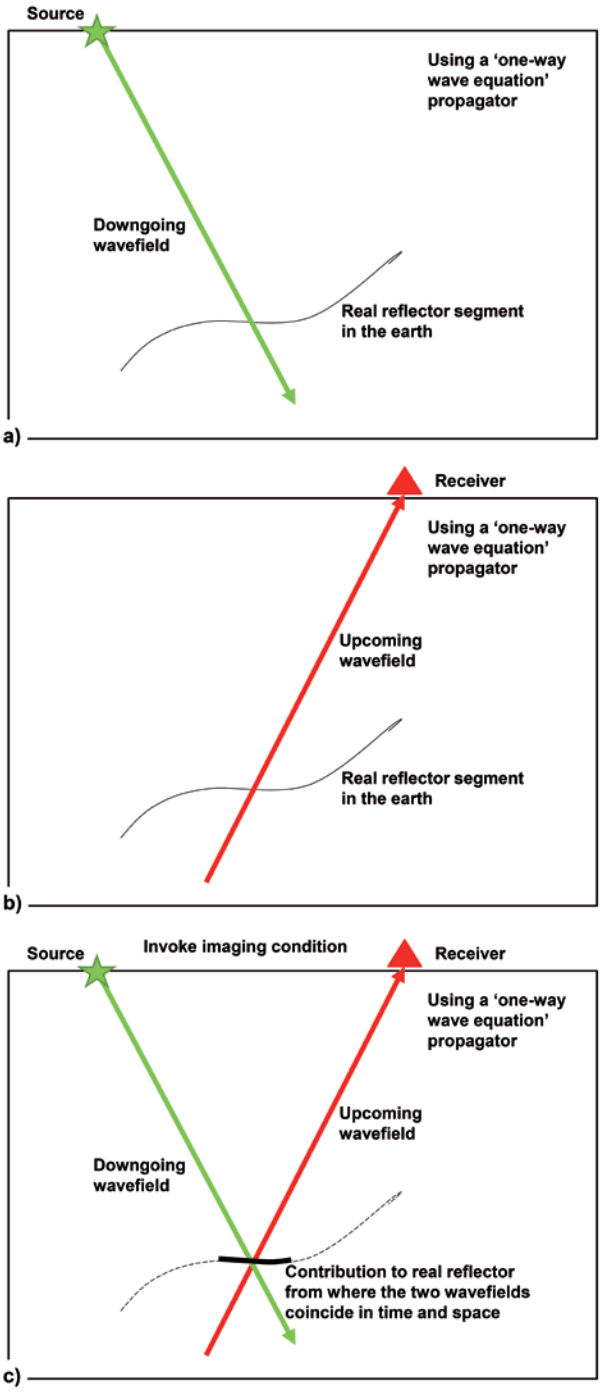

Figure 4 *One-way shot migration imaging condition for a simple reflector. a) Downgoing source-side wavefield for one-way propagation, b) Upcoming receiver-side wavefield, c) Imaging condition from multiplying both wavefields together to form a contribution to the final image.*

Imaging condition artefacts

For a one-way solution of the wave equation using a shot extrapolation migration scheme (Sava and Fomel, 2006), the procedure of multiplying the downgoing and upcoming

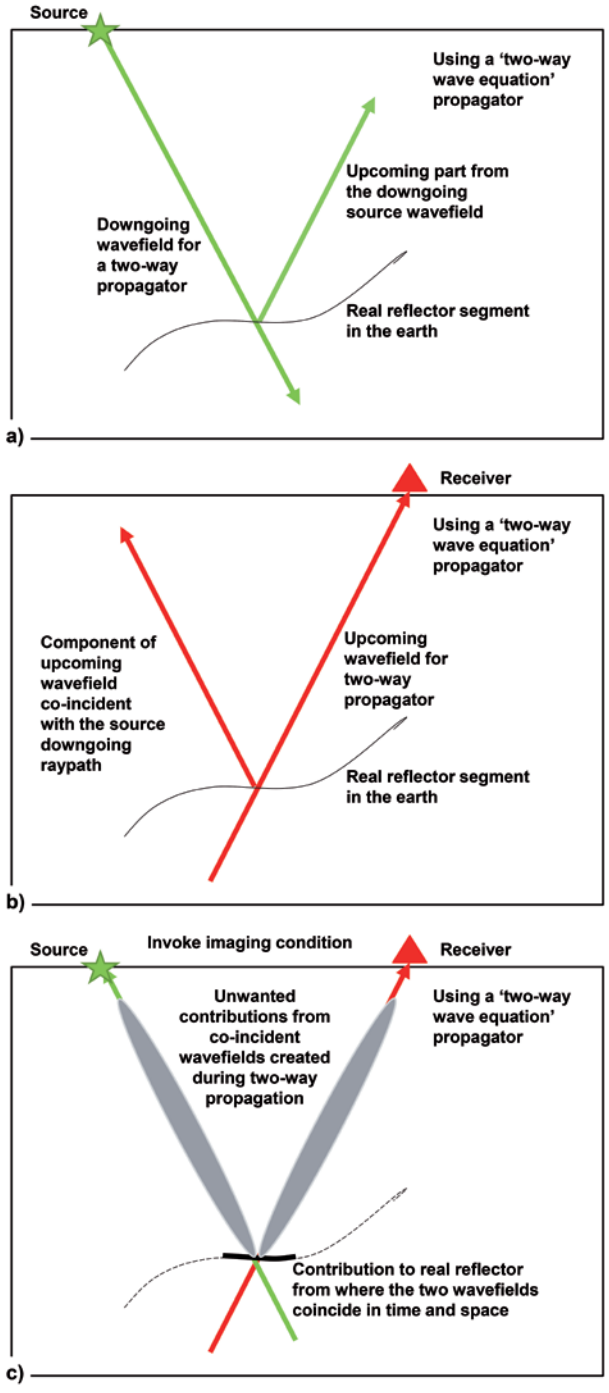

Figure 5 *Two-way shot migration imaging condition for a simple reflector. a) Downgoing source-side wavefield for two-way propagation – this has energy on the downgoing path, but also creates a contribution back up along the upgoing path. b) Upcoming receiver-side wavefield propagated back into the earth towards the reflector also reflects back upwards towards the source. c) Imaging condition from multiplying both wavefields together to form a contribution to the final image, but we also get an unwanted image contribution that has to be removed (the grey region along coincident portions of the ray paths).*

wavefields at each time step leads to an image of any simple reflections (Figure 4).

For a two-way solution of the wave equation, both the source-side and the receiver side wavefields can both travel upwards and downwards. This permits imaging of steep and complex geobodies via exploitation of double bounces and turning rays (e.g. Hale et al., 1992; Bernitsas et al., 1997; Cavalca and Lailly, 2005). Unfortunately, it also results in some unwanted side effects, such as spurious strong near-vertical artefacts emanating from overlapping downgoing and upcoming wavepaths, lateral amplitude terminations on strong vertical velocity boundaries (localized edge effects), and laterally mispositioned double bounce arrivals (e.g. when we have significant error in the anisotropy parameters). Figure 5 indicates how and where some of these unwanted contributions can form. The majority of the background low-frequency smear (the grey regions in Figure 5c) is often removed with filtering (e.g. in the KxKy domain). These artefacts typically only persist down to a depth where we encounter the first strong velocity contrasts (where the critical angle may be reached). Here, one side or the other (from the source and receiver wavefields) fails to penetrate below that depth for certain angles, hence this class of artefacts is reduced. Some of these artefacts can be removed by modifying the imaging condition by employing directional filters at each time propagation step (Poynting vector filtering: Yoon and Marfurt, 2006) but this approach is computationally expensive.

This procedure is shown in more detail in Figures 6 and 7. Figure 6a shows the result of migrating a single shot gather, where a strong near-vertical artefact is produced – outlined in yellow (corresponding to the unwanted grey smears of Figure 5c). After migrating all shots and summing their contributions, a final image is produced (Figure 6b) where most of the artefacts have been cancelled, and the background low frequency-wavenumber smear has also been removed by filtering. Figure 7 shows several images for the downgoing and upcoming wavefields for individual time steps in the propagation process, for the shot record migrated in Figure 6a. In these images, the red-and-black wavefront is the downgoing forward modelled source wavefield. Superimposed on the figure is the corresponding upcoming back-propagated receiver wavefield (in black-and-white). At any given propagation time step, where these two wavefields overlap with significant amplitude, we will obtain a contribution to the final image via their multiplication. A summation over all these multiplied time frames is then performed to produce the image contribution from this shot. The position of the strong artefact highlighted in Figure 6a is overlain on each of the wavefield snapshots, and it can be seen that the strong coincident energy of the downgoing and upcoming wavefields builds to form this unwanted energy in the series of time frames leading down to the reflector at 3km depth (corresponding to about 1.94s two-way time for the offset in the shot gather shown).

Deghosting imaging conditions

There has been much recent development in the de-ghosting of marine surface-tow seismic data, whereby the interference patterns of the source-side and receiver-side sea-surface downgoing reflections (ghosts) are suppressed (e.g. Carlson,

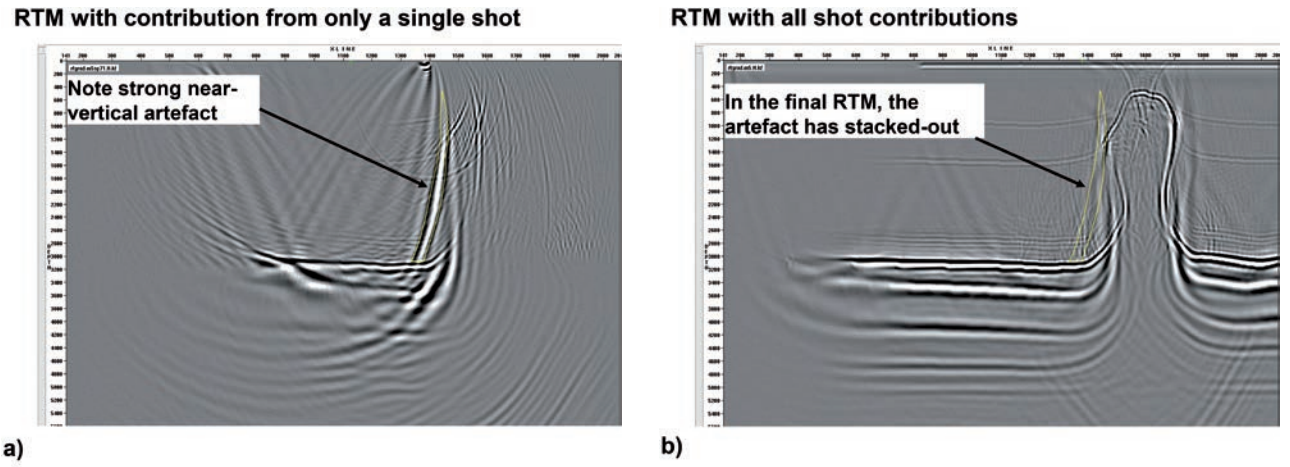

Figure 6 *a) The migration of a single shot record from synthetic modelling over a salt diapir, gives rise to an artefact (outlined in yellow). This artefact corresponds to the grey unwanted regions of Figure 5c. Some of these artefacts will cancel when added to the contribution of many adjacent shot records (as shown in 6b).*

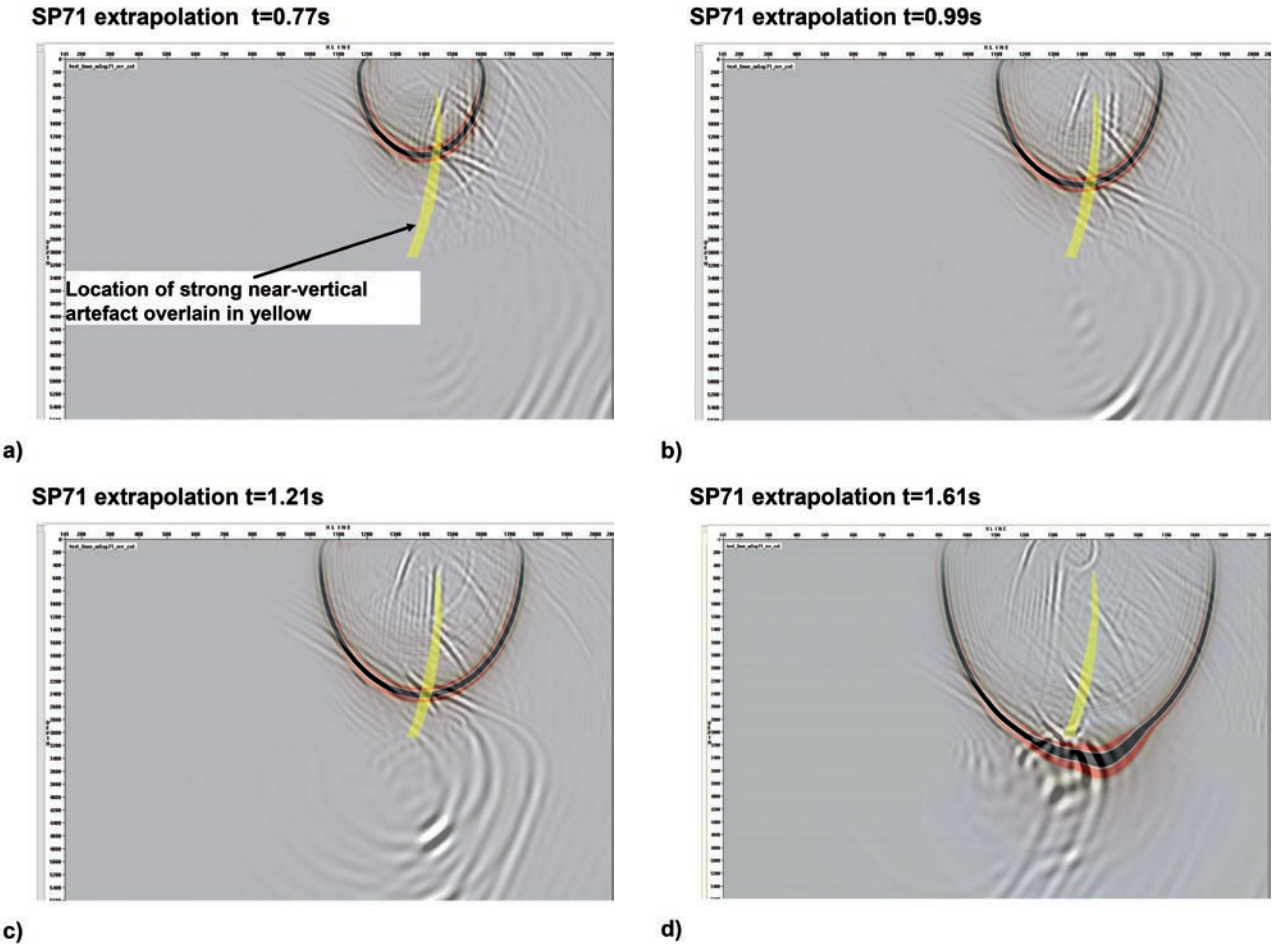

Figure 7 *The origin of this strong artefact seen in Figure 6a is highlighted in the wavefield propagation snapshots at times t = 0.77s, 0.99s, 1.21s, 1.61s (a, b, c, d, respectively).*

2007; Zhou et al., 2012). On the receiver side, the seismic signal we wish to process is the upcoming energy, but from the sea surface there is always a reverse polarity downgoing reflected copy of this signal (which becomes more coherent and pernicious with calmer weather, as the sea surface is then more mirror-like).

By exploiting the upcoming and downgoing aspects of two-way wavefield extrapolation migration (such as RTM), both the source and receiver ghost effects can be incorporated into the imaging condition in an attempt to deconvolve their interference effects during migration (e.g. Soubaras, 2010; Zhang et al., 2012).

Shot record extended imaging conditions

Each of the elemental sub-images resulting from the wavefield-extrapolation migration of an individual shot-record only contains a zero-offset trace: there is no inherent pre-stack gather resulting from this process. The correlation imaging condition only produces the image, not the gathers. Hence, to create a gather (say for use in subsequent velocity analysis or an AVA study) we need to invoke some additional computational techniques.

The most widely used of these methods is called an extended imaging condition. The idea in an extended imaging condition is to shift the downgoing and upcoming 3D wavefield volumes with respect to each other just before they are multiplied together at each propagation time step. These shifted product volumes are then summed as before to form the shifted image contribution from this particular shot record. This shifting procedure is repeated several times, so that we end-up with many 3D imaged volumes for each shot (one for each shift value), rather than a single image volume for the shot.

If we re-sort these shift-volumes into gathers (where the horizontal axis is the shift value), then we now have a pre-stack gather that can be used for velocity analysis and further post-processing prior to stack (the theory behind this technique is a form of interferometry). The shifting can be done in four different ways: laterally in the inline direction, laterally in the crossline direction, vertically in depth, or finally, in propagation time. It could also be done in depth with respect to the reflector normal (in other words, the vector represented by the inline, crossline, and vertical components), and this vector azimuth-angle gather can be computed from the inline and crossline shift results. The history of these extended imaging condition techniques dates back to focusing analysis in 2D preSDM (Faye and Jeannot, 1986; Audebert and Diet, 1990; MacKay and Abma, 1992) through to the more recent works of Ricket and Sava, 2002; Sava and Fomel, 2003; 2006; Biondo and Symes 2004; and Xu et al., 2010, among others.

The basic shift-gather is not intuitively very useful, but they can be converted into subsurface 'true' angle gathers via various transforms. However, all this shifting and transforming can suffer from aliasing of the underlying data due to poor sampling, most commonly in the crossline direction (Zhou et al., 2011). If we use a lateral inline or crossline shift, then the extended imaging condition gathers are called sub-surface-offset gathers, and if we shift in propagation time, they are called time-shift (or delay-time) gathers. Either can be converted to angle gathers ready for residual-moveout (RMO) picking and velocity updating, or post-processing, etc. Some authors prefer to use the propagation time delay gathers, as these are thought to be less prone to aliasing induced error. These time shift gathers are converted to angle gathers via a tau-p transform and a velocity scaling procedure.

Figure 8a shows an RTM time shift gather from the flank of a salt diapir. The horizontal axis corresponds to the degree of time delay relative to the basic (zero shifted) conventional imaging condition. The central trace in the time-shift gather (lag=0) is simply the migrated trace from the conventional RTM image. Shifting to positive or negative lags produces the traces on either side, and as these delays are progressive, the overall

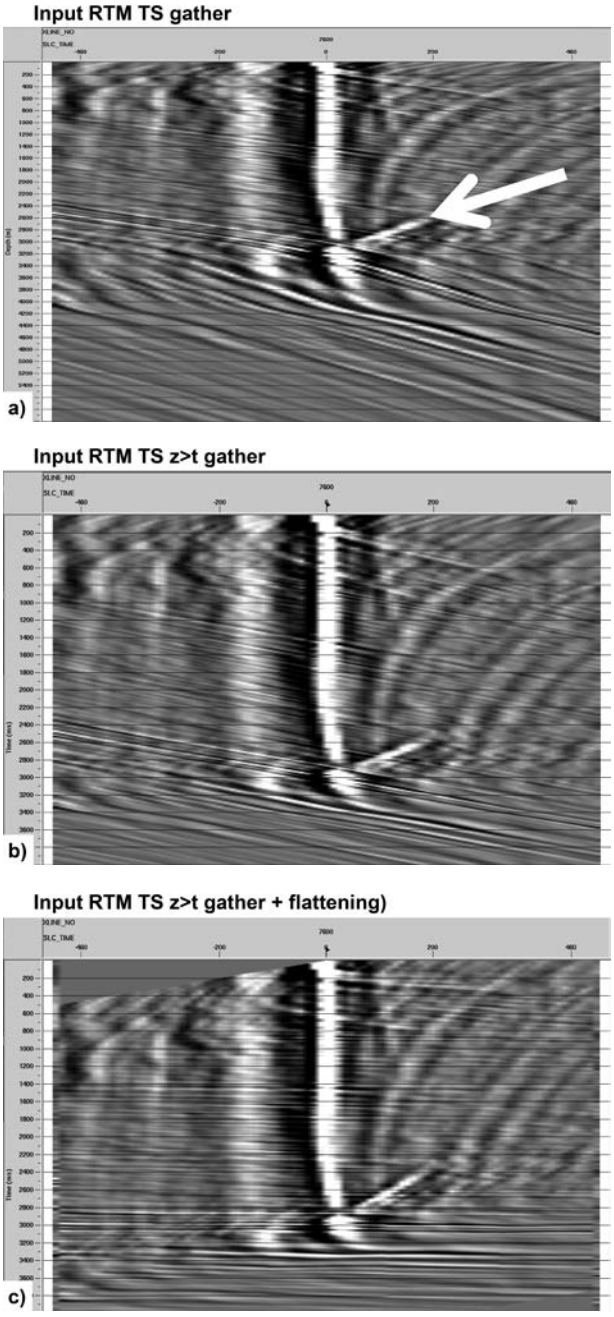

Figure 8 *a) The time shift gather at the location indicated by the yellow arrow in Figure 10b. The central trace from this gather (at shift=0) is the actual seismic trace at that location (as seen in Figure 10a). Shifting the wavefield to slightly earlier times or slightly later propagation times prior to forming the image produces the trace to either side of the central zero-shift trace. This results in the sloping appearance of events in the time-shift gather. The small segment of 'uphill' trending energy (indicated by the white arrow) is non-physical and needs to be removed, as does the low-frequency vertical event on and near to the zero lag trace. b) Converting the vertical axis from depth to time makes the sloping events appear linear, as velocity model distortion is removed. c) Rotating in accordance to the shift travel time, makes the gathers look flat, so that in a subsequent tau-p transform the p=0 trace will correspond to zero angle of incidence at a reflector.*

appearance of the time-shift gather is that of sloping events. The vertical low frequency 'stripe' (on and around the central zero lag trace) results from the two-way wave equation artefact of Figure 5c. It is interesting to note that this low frequency effect will only occur if the velocity model is good. If it was far from the real earth velocity structure, then the forward modelled downgoing wave would seldom be coincident with the real receiver wavefield. As mentioned previously, these artefacts only persist down to a depth where the critical angle is reached, typically at a large vertical velocity contrast event; in this case the salt-sediment interface. In Figure 8b, the data are stretched vertically from depth to time so as to remove velocity-induced distortion of otherwise linear trending events, and then rotated to make them suitable for transformation to the angle domain (Figure 8c). Figure 9 shows the data converted via a tau-p transform (and velocity scaling) to produce angle gathers, which can be muted to remove unwanted energy prior to conversion back to the time shift domain (Figure 9b).

An example of such processing is shown in Figure 10. The first image is an unfiltered RTM result for the shallow seismic section showing the low-frequency background energy (discussed in Figure 5c). The general background low frequency noise is removed with a KxKy filter (figure 10b). However, we still see a strong event emanating from the left flank of the salt dome which is clearly non-geological. Such

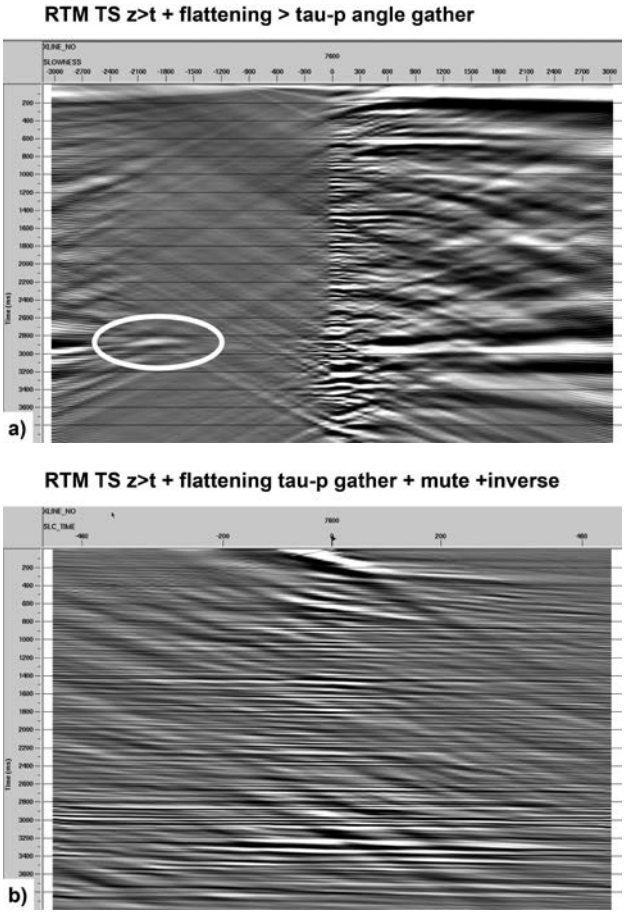

Figure 9 *a) Tau-p transform of the time-shift gather shown in Figure 8c: energy to the left of the centre corresponds to non-physical events thus is unwanted: the event circled in white corresponds to the dipping segment indicated by the arrow in Figure 8a. b) The time-shift gather after tau-p filtering and conversion back to the time domain via inverse-tau-p transform.*

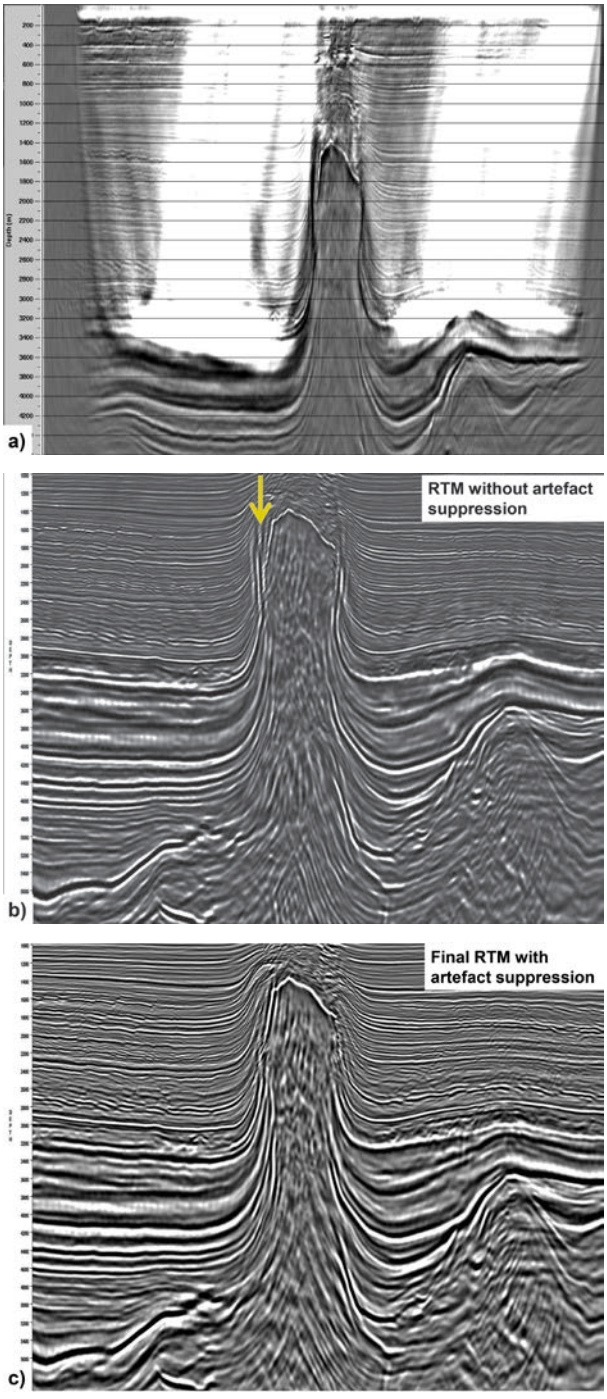

Figure 10 *a) Shallow section from the RTM image prior to filtering the back-scattered noise; b) Deeper section showing near-vertical RTM artefact emanating from a strong reflector termination (indicated with the yellow arrow). This image is taken from an early stage of the velocity model building. c) Image from later stage in the model building after filtering of RTM angle gathers (as shown in Figure 9b). (From Jones and Davison, 2014: GXT RTM image shown courtesy of Talisman Sinopec Energy UK and partners GdF-Suez, EON and Idemitsu. Input data courtesy of CGG).*

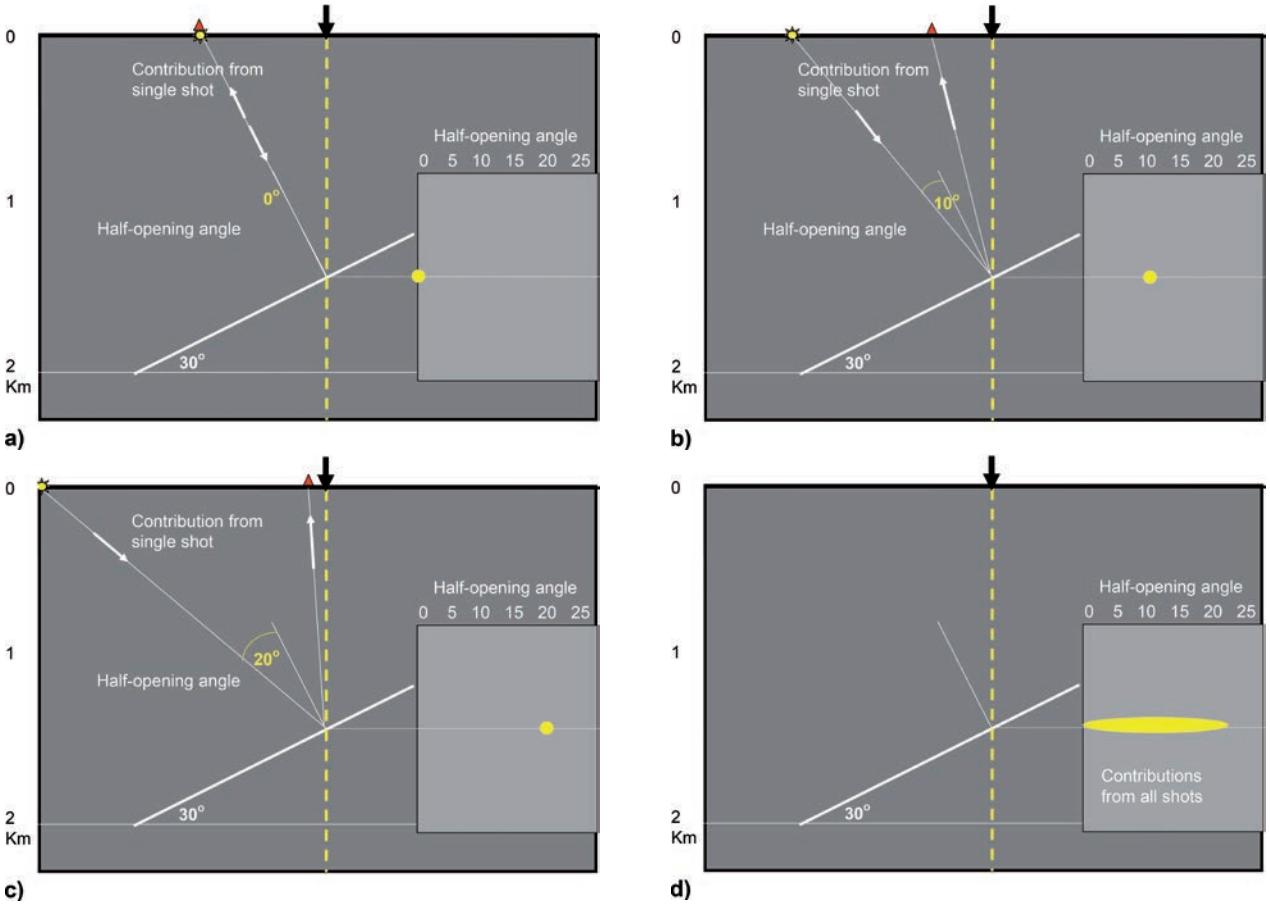

Figure 11 *a)-c): Contributions to the image at a specific specular point on a subsurface reflector from neighbouring shots and receivers for opening angles 0°, 10°, and 20° respectively. The angle gathers are formed by merging contributions from several shots (d).*

unwanted energy can be removed by filtering of the RTM angle gathers (e.g. Kaelin and Carvajal, 2011; Xie et al., 2012), producing an acceptable image (Figure 10c).

Poynting vector angle gathers

The Umov-Poynting vector (e.g. Yoon et al., 2004; Zhang and McMechan, 2011) describes the direction a wavefront is travelling in. In order to determine this information, we need to take the spatial derivative of the wavefield at all times (the divergence) and the temporal derivative at all spatial locations. This will tell us which way every point on the wavefront is travelling at all times. Once we have computed the RTM image (using an imaging condition as described previously), we use the Poynting vector to determine the angular contribution a given input shot gather has to each point in the subsurface in this image. Combining the contributions for all input shots permits building of angle gathers for each subsurface location (e.g. He, et al., 2012).

Figure 11 depicts a subsurface reflection point on a 30^0 dipping horizon where the vertical dashed line intersects the horizon. Any given incident (opening) angle at this subsurface point will only be illuminated by a single shot and receiver pair, as indicated in Figures 11a-c for opening angles 0^0, 10^0, and 20^0 respectively. We can separate-out this part of the RTM image using the Poynting vector information, so as to obtain the angular contribution at this point from that shot gather. Combining information from neighbouring shots (Figure 11d) builds-up the full angle gather which can facilitate analysis of the subsurface incident angles. The angle described here is not the reflector dip, but rather the opening angle at the reflector (the angle of incidence with respect to the normal to the reflector).

The phase bias of the imaging condition

The sum of migration operators forms the impulse response. If velocity changes across the survey, then each operator has a different shape, and the sum of operators (the impulse response) has a different asymmetric shape. Even for a time migration where the individual operators are symmetric (as they assume a locally 1D earth model) the sum of the differing but individually symmetric operators will be asymmetric (e.g. Jones, 2010). The operators we are summing are however acausal (as they emanate upwards from the scattering point, with no contributions from below the reflector) hence they will have a systematic phase bias in the resulting sum of operators. For a real reflecting event, we would not expect to have any energy appearing above the reflector, as that is non-physical (acausal), rather we only expect to see energy once it has reflected (either at the horizon or below it). To assess the phase behaviour of

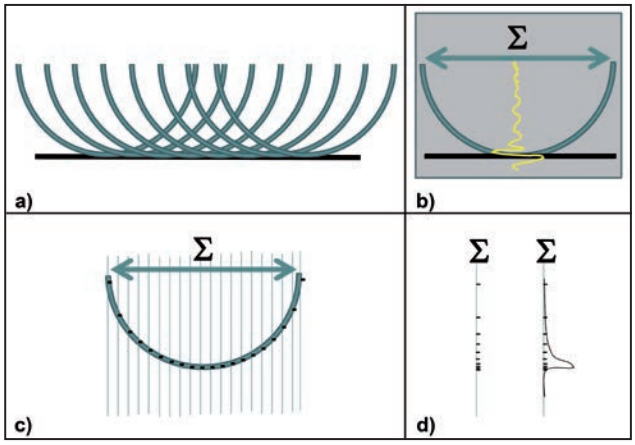

Figure 12 *a) In migration with constant velocity, a flat layer can be built from the laterally shifted sum of copies of the operator. So, a way of producing the response for a single point on this flat layer, would be to take a single operator, and laterally sum all the samples to produce a single trace in the centre of the operator (b). If the wavelets on the individual traces were spikes (c), then the summation of traces in the operator would not produce the desired spike at the reflector location, but rather a strange wavetrain extending upwards from the reflector (d): on the left is shown the individual spikes on the trace, and to the right is how this might appear as a continuous waveform.*

summing such operators it is instructive to see how we build the response of a flat layer.

Figure 12 showns the mechanism for the origin of this phase distortion. The seismic image of a flat layer underlying a constant velocity medium is constructed from the sum of laterally shifted copies of the same operator as indicated in Figure 12a. So, a way of producing the response for a single point on this flat layer is to take a single operator and laterally sum all its samples to produce a single trace in the centre of the operator (Figure 12b). Now consider the case where the wavelet on each individual trace of this operator prior to any summation has zero phase. We have to consider what happens to the phase of the resulting wavelet when we sum all those elemental zero phase wavelets. If the wavelets on the individual traces were spikes (Figure 12c) then the summation of traces in the operator would not produce the desired spike at the reflector location, but rather a strange wave-train extending upwards from the reflector (Figure 12d). In other words, it looks like an asymmetric acausal operator.

Consequently, the phase of the wavelet constituting the flat reflector, which comes from the immediate imaging condition in migration, is *not* zero phase, but it should be (assuming that we had performed conversion to zero-phase of the input data). Consequently, we correct it with what is called the derivative filter (as it has the same mathematical form as differentiation). This is also referred to as a rho filter.

Discussion

The final stage in migration, the imaging condition, builds the actual image. Depending on the migration technique used, this can produce either the image alone (as in WEM and RTM) or any combination of images and gathers (as in ray techniques). For the extrapolation methods we need additional steps to create gathers. Here, I have outlined the mechanics of these procedures, but I have not dwelt on aspects related to amplitude preservation, as that is beyond the scope of this work.

However, it should be recognised that it is at the imaging condition stage of the migration that we have the opportunity to obtain truly representative amplitudes if the imaging condition is dealt with appropriately (e.g. Lumley, 1989; Zhang et al., 2005; Zhang and Sun, 2009; Arntsen et al., 2010; Xu et al., 2010). In ray-based methods, the amplitude weights during the imaging phase have been well addressed for many years, and Kirchhoff amplitudes are considered reliable. However, as indicated in this brief overview, the imaging condition for wavefield extrapolation methods is difficult to execute in a stable but cost effective way with current computer resources, hence various compromises are typically made, especially in forming angle gathers.

Acknowledgements

My sincere thanks to Jacques Leveille, John Brittan, and Tony Martin for helpful suggestions for improvement of this work, to Mick Sugrue for producing the RTM movie snapshots and to ION for permission to publish.

References

Arntsen, B., Tantserev, E. and Amundsen, L. [2010] True-amplitude cross-correlation shot-profile imaging condition. *81st Annual International Meeting, SEG*, Expanded Abstracts, 3273-3277.

Audebert, F. and Diet, J.P. [1990] A focus on focusing. *52nd EAGE Conference & Exhibition*, Extended Abstracts, 107-108.

Bancroft, J.C. [1997] *A Practical Understanding of Pre/Poststack Vol.1*. SEG.

Bancroft, J.C. [2007] *A Practical Understanding of Pre/Poststack Vol.2 (Pre stack)*. SEG.

Baysal, E., Kosloff, D.D. and Sherwood, J.W.C. [1983] Reverse time migration. *Geophysics*, **48**, 1514-1524.

Bednar, J.B., Yoon, K., Shin, C. and Lines, L.R. [2003] One Way vs Two Way Wave Equation Imaging – Is Two-Way Worth It? *65th EAGE Conference & Exhibition,* Extended Abstracts, B11.

Bernitsas, N., Sun, J. and Sicking, C. [1997] Prism waves – an explanation for curved seismic horizons below the edge of salt bodies. *59th EAGE Conference & Exhibition,* Extended Abstracts.

Biondi, B. and Symes, W.W. [2004] Angle-domain common-image gathers for migration velocity analysis by wavefield-continuation imaging. *Geophysics*, **69**, 1283-1298.

Carlson, D. [2007] Increased resolution of seismic data from a dual sensor streamer cable. *74th Annual International Meeting, SEG,* Expanded Abstracts.

Cavalca, M., and Lailly, P. [2005] Prismatic reflections for the delineation of salt bodies. *72nd Annual International Meeting, SEG,* Expanded Abstracts.

Červený, V. [2001] *Seismic ray theory*. Cambridge University Press.

Claerbout, J.F. [1971] Toward a unifned theory of reflector mapping. *Geophysics*, **36**, no. 3, 467-481.

Faye, J.P. and Jeannot, J.P. [1986] Prestack migration velocities from depth focusing analysis. *56th Annual International Meeting, SEG,* Expanded Abstracts.

Fletcher, R.F., Fowler, P., Kitchenside, P. and Albertin, U. [2005] Suppressing artefacts in prestack reverse-time migration. *72nd Annual International Meeting, SEG,* Expanded Abstracts, 2049–2051.

Gray, S.H. [1992] Frequency-selective design of the Kirchhoff migration operator. *Geophysical Prospecting*, **40**, 565-572.

Gray, S. [2004] Gaussian beam migration of common-shot records. *71st Annual International Meeting, SEG,* Expanded Abstracts, 953-956.

Guitton, A., Kaelin, B. and Biondi, B. [2006] Least-square attenuation of reverse-time migration artefacts. *73rd Annual International Meeting, SEG,* Expanded Abstracts, 2348–2352.

Hale, D. [1991], Stable explicit depth extrapolation of seismic wavefields. *Geophysics*, **56**, 1770-1777.

Hale, D., Hill, N.R. and Stefani, J. [1992] Imaging salt with turning seismic waves. *Geophysics*, **57**, no.11, 1453-1462.

He, Y, Yoon, K., Cai, J., Yeh, A., Wang, B. and Li, Z. [2012] Practical Aspects of Subsalt Tomography Using Reverse Time Migration Based Angle Gathers. *74th EAGE Conference & Exhibition*, Extended Abstracts.

Hemon, C. [1978] Equations d'onde et modeles. *Geophysical Prospecting*, **26**, 790–821.

Hill, N.R. [1990] Gaussian beam migration. *Geophysics*, **55** (11), 1416–1428.

Jeannot, J.P. [1988] Full prestack versus shot record migration: Practical aspects. *58th Annual International Meeting, SEG,* Expanded Abstracts.

Jones, I.F. [2010] *An introduction to velocity model building*. EAGE, Houten.

Jones, I.F. and Davison, I. [2014] *Seismic imaging in and around salt bodies*. Accepted for SEG Interpretation.

Jones, I.F. and Lambaré, G. [2003] Wave equation versus ray based imaging. *First Break*, **21** (2), 11–13.

Jones, I.F., Bloor, R.I., Biondi, B. and Etgen J.T. [2008] Pre-stack depth migration and velocity model building. *SEG Geophysics Reprints*, **25**, Series Editor: Michael A. Pelissier, 840 pages.

Kaelin, B. and Carvajal, C. [2011] Eliminating imaging artifacts in RTM using pre-stack gathers. *82nd Annual International Meeting, SEG,* Expanded Abstracts.

Koren, Z., Ravve, I., Bartana, A. and Kosloff, D. [2007] Local angle domain in seismic imaging. *69th EAGE Conference & Exhibition,* Extended Abstracts, P287.

Leveille, J.P., Jones, I.F., Zhou, Z-Z., Wang, B., Liu, F. [2011] Subsalt Imaging for Exploration, Production and Development. A Review. *Geophysics*, **76**, WB3–WB20.

Liu, F., Zhang, G., Morton, S.A. and Leveille, J.P. [2011] An effective imaging condition for reverse-time migration using wavefield decomposition. *Geophysics*, **76**, S29–S39.

Loewenthal, D., Stoffa, P.L. and Faria, E.L. [1987] Suppressing the unwanted reflections of the full wave equations. *Geophysics*, **52**, 1007–1012.

Lumley, D.E. [1989] Kirchhoff prestack depth migration: Imaging conditions and amplitude recovery. *59th Annual International Meeting, SEG,* Expanded Abstracts, 1336–1339.

MacKay, S. and Abma, R. [1992] Imaging and velocity estimation with depth-focusing analysis. *Geophysics*, **57**, 1608–1622.

McMechan, G.A. [1983] Migration by extrapolation of time-dependent boundary values. *Geophysical Prospecting*, **31**, 413–420.

Nemeth, T., Wu, C. and Schuster, G.T. [1999] Least-squares migration of incomplete reflection data. *Geophysics*, **64**, 208–22.

Popov, M.M. [1982] A new method of computation of wave fields using Gaussian beams. *WaveMotion*, **4**, 85–97.

Rickett, J. and Sava, P. [2002] Offset and angle-domain common image-point gathers for shot-profile migration. *Geophysics*, **67**, 883–889.

Sava, P. and Fomel, S. [2003] Angle-domain common-image gathers by wavefield continuation methods. *Geophysics*, **68**, 1065–1074.

Sava, P. and Fomel, S., [2006] Time-shift imaging condition in seismic migration. *Geophysics*, **71**, S209–S218.

Sava, P., and Poliannikov, O. [2008] Interferometric imaging condition. *Geophysics,* **73**, S47–S61.

Schleicher, J., Costa, J.C., Novais, A. [2007] *A Comparison of Imaging Conditions for Wave-Equation Shot-Profile Migration.* http://www.portalabpg.org.br/PDPetro/4/resumos/4PDPETRO_1_2_0533-1.pdf, accessed May 2014.

Schuster, G. [1997] *Acquisition footprint removal by least square migration.* 1997 Annual UTAM Report, 73–99.

Soubaras, R. [2010] Deghosting by joint deconvolution of a migration and a mirror migration. *81st Annual International Meeting, SEG,* Expanded Abstracts, 3406–3410.

Whitmore, N.D. [1983] Iterative depth migration by backward time propagation. *53rd Annual International Meeting, SEG,* Expanded Abstracts.

Williamson, P., Wang, B., Bevc, D., Jones, I.F. [2010] Full wave-equation methods for complex imaging challenges. *The Leading Edge*, **29** (3), 264–268.

Xie, J., Whiteside, W., and Wang, B. [2012] Remove RTM Artifacts Using Delayed Imaging Time Gathers. *83rd Annual International Meeting, SEG,* Expanded Abstracts.

Xu, S., Zhang, Y. and Tang, B. [2010] 3D common image gathers from reverse time migration. *81st Annual International Meeting, SEG,* Expanded Abstracts, 3257–3262.

Yoon, K., Marfurt, K.J. and Starr, W. [2004] Challenges in reverse-time migration. *75th Annual International Meeting, SEG,* Expanded Abstracts, 1057–1060.

Yoon, K. and Marfurt, K.J. [2006] Reverse-time migration using the Poynting vector. *Exploration Geophysics*, **37**, 102–107.

Zhang, Q. and McMechan, G.A. [2011] Direct vector-field method to obtain angle-domain common image gathers for isotropic acoustic and elastic reverse-time migration. *Geophysics*, **76**, WB135–WB149.

Zhang, Y., Roberts, G. and Khalil, A. [2012] Compensating for source and receiver ghost effects in reverse time migration. *83rd Annual International Meeting, SEG,* Expanded Abstracts.

Zhang, Y. and J. Sun, [2009] Practical issues of reverse-time migration: True amplitude gathers, noise removal and harmonic-source encoding. *First Break*, **26**, 19–25.

Zhang, Y., Zhang, G. and Bleistein, N. [2005] Theory of true amplitude one-way wave equations and true amplitude common-shot migration. *Geophysics*, **70**, E1–E10.

Zhou, Z.Z., Howard, M. and Mifflin, C. [2011] Use of RTM full 3D subsurface angle gathers for subsalt velocity update and image optimization. Case study at Shenzi field, *Geophysics*, **76**, WB27–WB39.

Zhou, Z.Z., Cvetkovic, M. Xu, B. and Fontana, P. [2012] Analysis of a broadband processing technology applicable to conventional streamer data. *First Break*, **30** (10), 77–82.

Received: 3 July 2014; Accepted: 30 July 2014.
doi: 10.3997/1365-2397.2014017

